Geoderma 249–250 (2015) 28–39

Contents lists available at ScienceDirect

Geoderma

journal homepage: www.elsevier.com/locate/geoderma

Experimental aluminization of vermiculite interlayers: An X-ray diffraction perspective on crystal chemistry and structural mechanisms

Bruno Lanson [a,b,*], Eric Ferrage [c,d], Fabien Hubert [c,d], Dimitri Prêt [c,d], Louis Mareschal [e,f], Marie-Pierre Turpault [e], Jacques Ranger [e]

[a] Univ. Grenoble Alpes, ISTerre, F-38041 Grenoble, France
[b] CNRS, ISTerre, F-38041 Grenoble, France
[c] Univ. Poitiers, IC2MP, F-86000 Poitiers, France
[d] CNRS, IC2MP, F-86000 Poitiers, France
[e] INRA, Biogéochimie des Ecosystèmes Forestiers, F-54280 Champenoux, France
[f] CIRAD, Eco & Sols, F-34060 Montpellier, France

ARTICLE INFO

Article history:
Received 21 October 2014
Received in revised form 8 January 2015
Accepted 4 March 2015
Available online xxxx

Keywords:
Hydroxy-interlayered vermiculite
Hydroxy-interlayered smectite
Interlayer Al
Clay mineral aluminization
X-ray diffraction
Acid soils

ABSTRACT

Natural aluminization of swelling clay minerals is ubiquitous in acidic soils leading to the formation of hydroxy-interlayered (HI) minerals. This process has drawn special attention over the last 4–5 decades owing to the negative impact on soil fertility of the induced reduction of cation exchange capacity. Combination of chemical analyses and of X-ray diffraction profile modeling on a series of experimentally self-aluminized samples aimed at an improved description of HI minerals and more especially of their interlayer crystal chemistry. Both exchangeable alkali cations and hydroxy (Al, Fe) cations coexist within HI vermiculite interlayers. The latter form discontinuous gibbsite-like interlayer sheets with ~15% completeness, despite layer-to-layer distances similar to that of chlorite. From charge compensation considerations, the isolated hydroxy (Al, Fe) cation clusters bear ~1.5 positive charges per cation. Analysis of X-ray diffraction data indicates that aluminization of initially swelling interlayers is a layer-by-layer process leading to mixed layers composed of randomly interstratified swelling and aluminized layers, all aluminized layers likely hosting a similar number of hydroxy (Al, Fe) cations along the aluminization process. This model contradicts the widely accepted description of HI minerals as a solid solution between expandable 2:1 clay and aluminous chlorite end-members. As a consequence, the proportion of HI layers in the mixed layer is a robust estimate of aluminization progress and both the amount of extractible (Al, Fe) and the extent of CEC decrease are positively correlated to this essential parameter.

1. Introduction

Natural aluminization of clay minerals has been reported in various soil orders, mostly in acidic environments (Rich, 1968). In such environments, dissolution of minerals, including clay minerals, releases aluminum to soil solution, this aluminum being subsequently fixed as $Al[(OH)_x,(H_2O)_y]^{3-x}$ polymers in initially swelling clay interlayers to form hydroxy-interlayered (HI) minerals (Barnhisel and Bertsch, 1989). HI minerals can develop under tropical (Bortoluzzi et al., 2008), temperate (Bain et al., 1990; Righi, 1993; Righi et al., 1986; Righi and Meunier, 1991; Wilson et al., 1984), boreal (Tolpeshta et al., 2010), or alpine (Egli et al., 2001, 2003, 2007) climates. Compared to the original swelling clays, the cation exchange capacity (CEC) of HI minerals is significantly reduced together with their ability to expand upon incorporation of organic polar molecules (Meunier, 2007). Over the last 4–5 decades, aluminization of swelling minerals has thus drawn a lot of attention owing to the negative impact of the CEC loss on soil fertility, compared to initial swelling minerals (Barnhisel and Bertsch, 1989). In particular, chemical parameters controlling the aluminization process have been sought and the crystal structure and interlayer composition of these minerals investigated (see for example the reviews of Barnhisel and Bertsch, 1989, and of Rich, 1968), primarily from experimental studies owing to the intrinsic heterogeneity of natural HI minerals. As discussed in detail by Mareschal et al. (2009), two main reaction pathways have been used to form HI minerals. Addition of Al (and possibly other metal cations) solutions in suspensions of swelling clay minerals (smectite or vermiculite) allowed probing a variability of parameters (initial layer type, OH:Al ratio, aging time, solid:solution ratio, ionic strength, …). On the other hand, self-aluminization fed by the partial dissolution of swelling clay minerals in acidic solutions appears to mimic more realistically HI mineral formation processes occurring in acidic soils (Vicente et al., 1977).

Relying mainly on their X-ray diffraction (XRD) signature, HI minerals have been described as discrete (periodic) phases from the solid solution extending from pure swelling clays to pure aluminous chlorite

* Corresponding author at: Univ. Grenoble Alpes, ISTerre, F-38041 Grenoble, France.
E-mail address: Bruno.lanson@ujf-grenoble.fr (B. Lanson).

http://dx.doi.org/10.1016/j.geoderma.2015.03.005
0016-7061/

(Barnhisel and Bertsch, 1989). According to this model, hydroxy-interlayering affects all interlayer spaces in a similar way, and the contrasting diffraction signatures (mainly the position of the 001 reflection) upon a variety of treatments (air-drying, interlayer cation saturations, heating, etc.) depend essentially on the interlayer occupancy by hydroxy Al cations. Both HI smectites and vermiculites possess a ~14.2 Å layer-to-layer distance that remains stable upon a broad range of relative humidity conditions and with a variety of interlayer cations. HI vermiculite layers partially collapse upon heating at 300 °C, however, whereas HI smectite layers collapse upon K-saturation is enhanced by heating to moderate temperature (Meunier, 2007). HI smectite layers exhibit also limited swelling upon ethylene glycol solvation (Meunier, 2007). Consistently, aluminization progress is described by the steady increase of hydroxy Al cation content in initially expandable interlayers, thus leading to the observed CEC reduction. Experimental formation of HI smectite and vermiculite indicates that interlayer occupancy, and the actual nature of the interlayer hydroxy Al cations, is controlled by the nature of the original 2:1 swelling clay (smectite or vermiculite), the OH:Al ratio in solution, and contact time (Brindley and Sempels, 1977; Carstea, 1968; Hsu and Bates, 1964; Rich, 1960; Sawhney, 1968; Schwertmann and Jackson, 1964; Veith, 1978). Despite the self-consistency of the dominant solid-solution model, crystal structure of HI minerals remains controversial, as their description as mixed layers containing both expandable and aluminous chlorite (with partial interlayer occupancy) layers accounts equally well for their XRD signature as proposed by Meunier (2007) consistent with previous reports (Cradwick and Wilson, 1978; Wilson, 1966). According to the latter model, aluminization progress results mainly from the compositional evolution of the mixed layer, that is from the relative proportions of expandable and HI layers, and to a minor extent from the interlayer occupancy of the latter layers.

The present work thus reports on the structural characterization of HI vermiculite at different stages of its experimental aluminization in acidic solution (Mareschal et al., 2009). Combination of chemical and thermal analyses, and of XRD profile modeling aimed specifically at an improved description of these mineral species and of their interlayer crystal chemistry.

2. Material and methods

2.1. Samples and experimental procedure

Samples whose structure is investigated in the present work were prepared by Mareschal et al. (2009). For their alteration experiments, these authors prepared a 200–400 μm size fraction from centimetric flakes of Santa Olalla reference vermiculite (Andalusia, Spain — de la Calle and Suquet, 1988) and Na-saturated it (Mareschal et al., 2009). Additional information about Santa Olalla vermiculite, including its behavior upon Mg-saturation and ethylene-glycol solvation, is available in de la Calle and Suquet (1988) and references therein. Conditions favorable to aluminization of vermiculite interlayers are detailed in the study of Mareschal et al. (2009). Briefly, experiments were performed at ~50 °C using series of flow-through reactors (4 mL in volume) by adding 4 mL of HCl (pH = 2.7) to ~250 mg of vermiculite at a 0.042 mL/min flow rate with continuous stirring. All experiments were performed simultaneously and stopped at different times (i.e., after 12, 36, 60, 96, 168, 240, and 672 h reaction times) to allow for liquid and solid analysis (Mareschal et al., 2009). Solid samples were washed several times with ultrapure water and dried before subsequent analysis. Scanning electron microscopy pictures of initial and altered vermiculite are available in Mareschal et al. (2009) together with XRD patterns of K-saturated and heated Santa Olalla vermiculite.

2.2. Thermal analysis

Thermal analysis of initial and most altered samples was performed in air with a NETZSCH Simultan STA 409 EP analyzer using a 10 °C/min heating rate over the 20–1100 °C temperature range. The weight loss due to structural water was measured by thermogravimetric analysis (TG) and differential scanning calorimetry (DSC) on ~20 mg Na-saturated (see below) samples equilibrated at ~40% RH.

2.3. Chemical analysis of the solids

For chemical analysis, a sample fraction was saturated with potassium to exchange all non-fixed interlayer species using a protocol similar to the one described below (see Section 2.4) for Na-saturation. Crystals (200–400 μm in size within the layer plane) were subsequently rinsed and oven dried for two days under primary vacuum, with a stepwise increase of temperature up to 160 °C. Crystals (>10 μm thick) were then mounted quickly on a glass slide using carbon adhesive tape and coated with a 30 nm thick layer of carbon. Quantitative chemical profiles were collected along the diameter of crystals with a JEOL 5600LV scanning electron microscope coupled with an Energy Dispersive X-ray (EDX) Spectrometer Bruker XFlash 4030 in stage rastering mode. An accelerating voltage of 15 kV, a working distance of 16.5 mm, a step size of 3 μm/point, a dwell time of 30 to 60 s/point, and a probe current of 1 nA were chosen to reach counting statistics allowing the quantitative treatment of individual EDX spectra. Quantification implied physical modeling of the background, Gaussian deconvolution of the spectra, and a standard-based XPP matrix correction (Prêt et al., 2010). The number of cations per formula unit (p.f.u.) was then calculated for fresh Santa Olalla vermiculite on a $O_{20}(OH)_4$ oxygen basis. For altered crystals, the number of cations was normalized on the same oxygen basis assuming an octahedral (Mg, Al, Fe, Mn) occupancy similar to that of the initial sample. Fe and Al atoms in excess, compared to the initial material, were then located in the altered vermiculite interlayers.

2.4. X-ray diffraction

For XRD analysis of altered solid, samples were saturated with sodium to exchange all non-fixed interlayer species. To do so, ~50 mg of solid was shaken mechanically for 12 h in 50 mL of 1 $mol \cdot L^{-1}$ NaCl solution at room temperature. The solid fraction was then separated by centrifugation and a fresh NaCl solution was added, the exchange procedure being repeated three times. Excess salt was removed by washing the solid three times in deionized water (resistivity >18 $M\Omega \cdot cm^{-1}$, 12 h contact), the solid fraction being separated by centrifugation. After drying, samples were gently crushed and passed through a 50 μm sieve. The resulting powders were then dispersed in deionized water and oriented slides prepared for all samples by drying at room temperature a clay slurry onto glass slides. XRD patterns were recorded with a Bruker D5000 diffractometer equipped with an Ansyco rh-plus 2250 humidity control device coupled to an Anton Paar TTK450 chamber, a SolX solid-state detector (Baltic Scientific Instruments) and CuKα radiation (λ = 1.5418 Å). Samples were equilibrated for a few hours at the desired relative humidity (RH) before data collection. Data were collected at room temperature over the 2–50° 2θ angular range using 6 s counting time per 0.04° 2θ step. Each pattern was recorded twice to ensure the stability of the hydration state. The divergence slit, the two Soller slits, and the antiscatter and resolution slits were 0.5°, 2.3°, 2.3°, 0.5° and 0.06°, respectively. For initial and most altered (672 h duration) samples, data were recorded at different RH values following the same sequence (40, 60, 80, 20, and 0% RH) to avoid a possible irreversible layer collapse under low RH conditions. Dry conditions (~0% RH) were obtained by evacuating the entire Paar chamber to a secondary vacuum (~10^{-4} Pa). For all samples, XRD patterns were collected under RH conditions (20% RH) selected to maximize both the layer-to-layer distance contrast between expandable and aluminized interlayers and the hydration homogeneity of expandable interlayers (see Section 3.2.1).

2.5. XRD profile modeling of 00ℓ reflections

XRD data were modeled using the algorithms developed initially by Drits and Sakharov (1976), Sakharov and Drits (1973), and Sakharov et al. (1982a, 1982b, 1983) and a trial-and-error approach similar to that involved in the multi-specimen method (Drits et al., 1997a; Sakharov et al., 1999a, 1999b). Modeling relies on the direct comparison of experimental XRD profiles with those calculated for a structure model. The optimum agreement between experimental and calculated XRD patterns is obtained by a trial-and-error procedure. Structure models include for each mixed layer, the number (limited to 3 in the present case), the nature and proportions of the different layer types and a statistical description of their stacking sequences (Reichweite parameter and junction probabilities). The approach is similar to that used by Ferrage et al. (2005a, 2005b, 2010, 2011) and Dazas et al. (2013, 2014, 2015) to refine the distribution of interlayer species (cations and H_2O molecules) within interlayers of expandable phyllosilicates. Sensitivity of the method allowed comparing successfully refined number and position of interlayer species with those derived from computational methods (Monte Carlo simulations in the Grand Canonical ensemble) and fine-tuning some of the interaction parameters used to compute details of smectite interlayer configuration. Mass absorption coefficient (μ^*) was set to 45 $cm^2 \cdot g^{-1}$, as recommended by Moore and Reynolds (1997). The *z*-coordinates for atoms of the 2:1 layers were set also as proposed by Moore and Reynolds (1997), as the *z*-coordinates of interlayer species for dehydrated (0 W-$d_{(001)}$ = 9.6–10.1 Å) and mono-hydrated (1 W-$d_{(001)}$ = 11.9–13.0 Å) Na-vermiculite layers. The *z*-coordinates of interlayer species for bi-hydrated and aluminized interlayers (2 W/HI-$d_{(001)}$ = 14.0–15.9 Å) were determined in the present study. The coherent scattering domain size along the **c***-axis was characterized by a mean value (N — Drits et al., 1997b) which was optimized. The σ_z parameter accounts for fluctuations of the layer-to-layer distance, and its value corresponds to the standard deviation of a Gaussian-type distribution centered on the mean layer-to-layer distance (Drits and Tchoubar, 1990; Ferrage et al., 2005a; Guinier, 1964; Sakharov and Lanson, 2013). The overall fit quality was assessed using the un-weighted Rp parameter (Howard and Preston, 1989) that is influenced mainly by misfits of most intense diffraction maxima such as the 001 reflection, which contains essential information on the proportions of the different layer types. The fitting procedure is described in detail by Ferrage et al. (2005a). Briefly, one periodic sequence of layers (0 W, 1 W, or 2 W-HI only) was used first to reproduce as much as possible of the XRD data. If necessary, extra contributions containing two or three layer types were added to the calculated profile. Up to five contributions (each with different proportions of layer types and/or ordering sequences) were necessary to reproduce some of the experimental patterns, because of structural heterogeneity leading to complex diffraction maxima having broad and asymmetric profiles. Layers with the same hydration state were assumed however to have identical parameters (identical values of the N and σ_z parameters, and atomic content) in the different mixed layers to minimize the number of adjustable parameters. Relative proportions of the different mixed layers and that of the different layer types in the mixed layers were considered as variables in the fitting procedure.

3. Results

3.1. Chemical analyses

Chemical profiles through vermiculite crystals did not show any statistically significant trend such as elemental enrichment towards the edges or the cores of analyzed crystals (data not shown). Individual analyses (500–1000 per sample), whose scatter along the profiles stays within the point-to-point analytical error, were thus averaged to calculate structural formulae for initial and altered material (Table 1). The average structural formula calculated for the initial material $[Me^{+}_{1.74}\ ^{IV}(Si_{5.48}Al_{2.52})\ ^{VI}(Mg_{4.94}Al_{0.40}Fe_{0.54}Mn_{0.02})\ O_{20}(OH)_4]$ (Table 1) is consistent with those reported in the literature for Santa Olalla vermiculite: $Me^{+}_{1.66}\ ^{IV}(Si_{5.44}Al_{2.56})\ ^{VI}(Mg_{5.18}Al_{0.12}Fe_{0.54}Ti_{0.16})\ O_{20}(OH)_4$ (de la Calle and Suquet, 1988), $Me^{+}_{1.82}\ ^{IV}(Si_{5.40}Al_{2.60})\ ^{VI}(Mg_{5.14}Al_{0.26}Fe_{0.52}Mn_{0.02})\ O_{20}(OH)_4$ (Pons et al., 1989), and $Me^{+}_{1.64}\ ^{IV}(Si_{5.66}Al_{2.34})\ ^{VI}(Mg_{4.92}Al_{0.60}Fe_{0.44})\ O_{20}(OH)_4$ (Argüelles et al., 2010), with similar octahedral and tetrahedral compositions, as well as similar overall layer charge deficit. In addition, TG analysis reveals the presence of two weight losses at ~100 and 205 °C most likely related to the release of interlayer H_2O molecules, whose actual content was thus quantified from the weight loss over the 50–250 °C range (11.66% — Fig. 1, Table 1). Initial vermiculite thus contains ~5.9 H_2O molecules (p.f.u.), that is ~3.4 H_2O molecule per interlayer cation.

After conversion to structural formulae calculated assuming a constant octahedral occupancy in both initial and altered materials, analyses performed on altered materials indicate the presence of a significant number of exchangeable alkali cations and of (Al, Fe) cations in excess. Among the various hypotheses tested, that of a constant octahedral occupancy in initial and altered materials was one of the very few allowing the calculation of realistic and electrically neutral structural formulae in contrast, for example, to the hypothesis of a constant tetrahedral composition. To allow for the calculation of the number of interlayer H_2O molecules from the weight loss over the 50–250 °C range (3.8 p.f.u.), molecular weight of altered vermiculite is computed assuming excess (Al, Fe) cations to be present as interlayer (Al, Fe)$(OH)_3$ species, and weight loss occurring over the 250–750 °C range can be interpreted as related to dehydroxylation of these species for altered sample. Dehydroxylation of the Mg-rich octahedral sheet of the 2:1 layer is minimal indeed at this temperature (Fig. 1). After correction for the weight loss observed for the initial sample (−1.06%), the additional weight loss observed for 672 h sample (−0.99%) is equivalent to the loss of ~0.50 H_2O molecules p.f.u., that is of ~0.75 H_2O molecule per excess (Al, Fe).

3.2. End-member solid analysis

To quantify the structural evolution of vermiculite as a function of alteration time, a first step consists in determining the hydration properties and interlayer structure of the two end-members (i.e., unaltered and most aluminized vermiculite layers). The understanding of hydration properties provides information on the RH conditions for which the layer-to-layer distance is most contrasting between the two end-members. This information is essential for the consistency of subsequent XRD profile modeling that allows determination of the proportion of the different layer types (unaltered and aluminized) from experimental XRD patterns and thus proper assessment of alteration progress (Ferrage et al., 2005c; Tertre et al., 2011). In addition, if the interlayer configuration (amount and position of interlayer species) of expandable vermiculite is known a priori (Ferrage et al., 2005b; Moore and Reynolds, 1997), that of aluminized interlayers needs to be determined as it represents an essential constraint to the modeling of XRD data.

3.2.1. "Hydration" behavior of the two end-members

In Fig. 2 XRD data are plotted as a function of RH for initial and most altered (672 h duration) samples after Na-saturation. In addition to information on the hydration state prevailing in smectite interlayers (Sato et al., 1992), or more precisely on the $d_{(001)}$ values as a function of RH, analysis of XRD patterns can provide information on the homogeneity of vermiculite interlayers through the calculation of 00ℓ reflection rationality (ξ parameter — Table 2). This parameter is calculated as the standard deviation of $\ell \times d_{(00\ell)}$ values for all measurable 00ℓ reflections over the 2–50° 2θ angular range, although some of these reflections may correspond to various hydration states.

For Na-saturated unaltered vermiculite (Fig. 2a), XRD patterns correspond to 1 W (20 and 40% RH, $d_{(001)}$ = 11.86 and 11.93 Å,

Table 1
Chemical composition of initial and altered samples calculated from chemical and thermal analyses (structural formulae calculated on a $O_{20}(OH)_4$ oxygen basis).

	Si (at. wt.%)	Al (at. wt.%)	Mg (at. wt.%)	Fe (at. wt.%)	Mn (at. wt.%)	K (at. wt.%)	Na (at. wt.%)	Wt. loss[a] 50–250 °C	Wt. loss[a] 250–750 °C
Santa Olalla (unaltered)	19.2	9.8	15.0	3.7	0.1	8.4	0.0	11.66%	1.06%
Altered 96 h	20.9	10.8	15.2	3.5	0.1	3.9	0.0	n.d.	n.d.
Altered 672 h	20.1	11.2	15.4	4.2	0.1	3.3	0.0	7.48%	2.05%

	^{IV}Si[b]	^{IV}Al[b]	^{VI}Mg[b]	^{VI}Al[b]	^{VI}Fe[b]	^{VI}Mn[b]	Oct. Occ.	$^{Int}(Al, Fe)$[b]	^{Int}K[b]	Tet. ch.[b]	Oct. ch.[b]	Layer ch.[b]
Santa Olalla (unaltered)	5.48	2.52	4.94	0.40	0.54	0.02	5.90	–	1.74	−2.52	+0.74	−1.78
Altered 96 h	5.70	2.30	4.80	1.08		0.02	5.90[c]	0.17	0.78	−2.30	+0.88	−1.42
Altered 672 h	5.66	2.34	5.00	0.88		0.02	5.90[c]	0.66	0.66	−2.34	+0.68	−1.66

Elemental proportions are given in atomic weight percent (at. wt.%) after normalization to 100% including oxygen atoms.
[a] Weight loss (Wt. loss) from the thermogravimetric analysis.
[b] Tetrahedral, octahedral and interlayer cations are differentiated with IV, VI, and Int. superscripts, respectively. Tetrahedral, octahedral and layer charges are noted as Tet. Ch., Oct. ch., and Layer ch., respectively.
[c] Octahedral occupancy (Oct. Occ.) in altered samples was supposed to be the same as that in the original sample.

respectively) and 2 W states (60 and 80% RH, $d_{(001)}$ = 14.82 and 14.85 Å, respectively) whereas both 0 W and 1 W states coexist at ~0% RH ($d_{(001)}$ = 9.81 and ~11.6 Å, respectively — Table 2, Fig. 2a). The observed transition between 1 W and 2 W states is consistent with that reported by de la Calle et al. (1978) for Na-saturated Santa Olalla vermiculite. These authors showed stable 1 W state for RH values ranging from 10 to 40% whereas 2 W state dominated over 60–100% RH range. Note however that the XRD pattern recorded at 60% RH displays a small peak at ~12.24 Å corresponding to a minor 1 W contribution (Fig. 2a). According to ξ parameter values, the most homogeneous structure is observed at 20% RH.

For the most altered sample (672 h), XRD profiles obtained after Na-saturation correspond to periodic structures with $d_{(001)}$ ~14.15–14.20 Å (Fig. 2b), consistent with that of HI vermiculite (Barnhisel and Bertsch, 1989), and minimal departure from rationality (ξ < 0.03 Å — Table 2) over the 20–80% RH range. Although no transition between different hydration states is observed, a small increase of the layer-to-layer distance may be observed, from 14.14 Å at 20% RH to 14.22 Å at 80% RH, indicative of an increased number of interlayer H_2O molecules (Ferrage et al., 2005a). At ~0% RH the structure appears heterogeneous with a $d_{(001)}$ value intermediate between the previous ones and that expected for 1 W structures and with a strongly irrational series of basal reflections (ξ = 0.728 Å — Table 2).

This qualitative observation of XRD data as a function of RH for the two end-members clearly shows that vermiculite structure is strongly affected by the experimental alteration. After alteration, vermiculite structure no longer exhibits the typical hydration behavior of expandable 2:1 clays, but rather presents a stable layer-to-layer distance, consistent with the presence of partially hydrated interlayer gibbsite-like sheets. This description allows determining also the relative humidity leading to a maximum layer-to-layer distance contrast between original and altered layers. At 20% RH, both initial and altered layers exhibit rational series of basal reflections characterized by low ξ values (0.006 and 0.024 Å, respectively — Table 2) and contrasting layer-to-layer distances (11.86 and 14.14 Å, respectively — Table 2).

3.2.2. Interlayer configuration of initial and aluminized vermiculite

3.2.2.1. Initial sample. XRD pattern recorded at 20% RH for the Na-saturated initial sample was fitted using the experimentally determined 2:1 layer chemistry and the interlayer configuration proposed by Moore and Reynolds (1997) for 1 W layers (Fig. 3a, Table 3). A main structure overwhelmingly dominated by 1 W layers randomly interstratified (Reichweite parameter R = 0) with a marginal amount of 0 W layers (1%) allows reproducing most of XRD data. A second mixed layer (R = 0) was necessary to account for the misfit observed on the tails

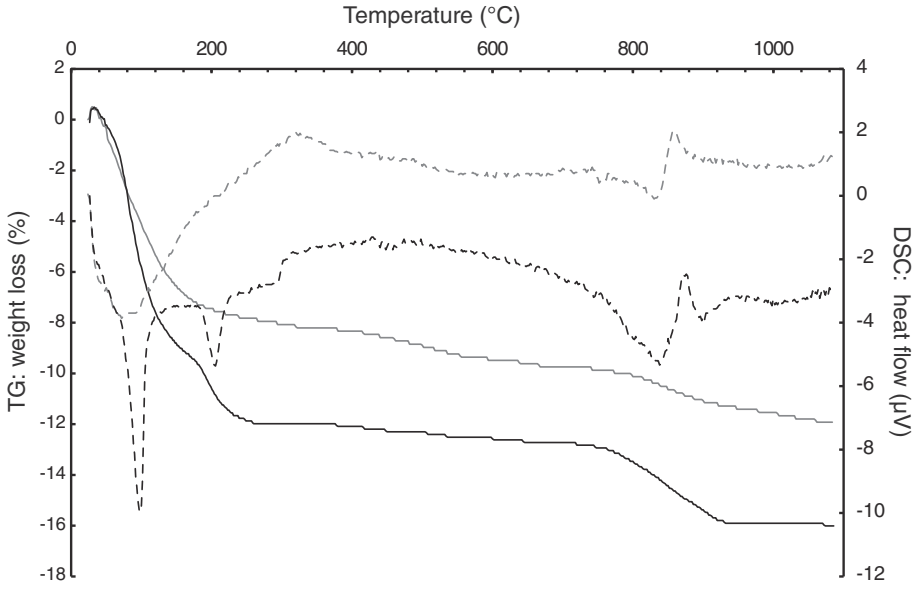

Fig. 1. Experimental thermogravimetric analysis (TG) and differential scanning calorimetry (DSC) obtained for the initial and the altered for 672 h samples (black and gray lines respectively). TG and DSC curves are shown as solid and dashed lines, respectively.

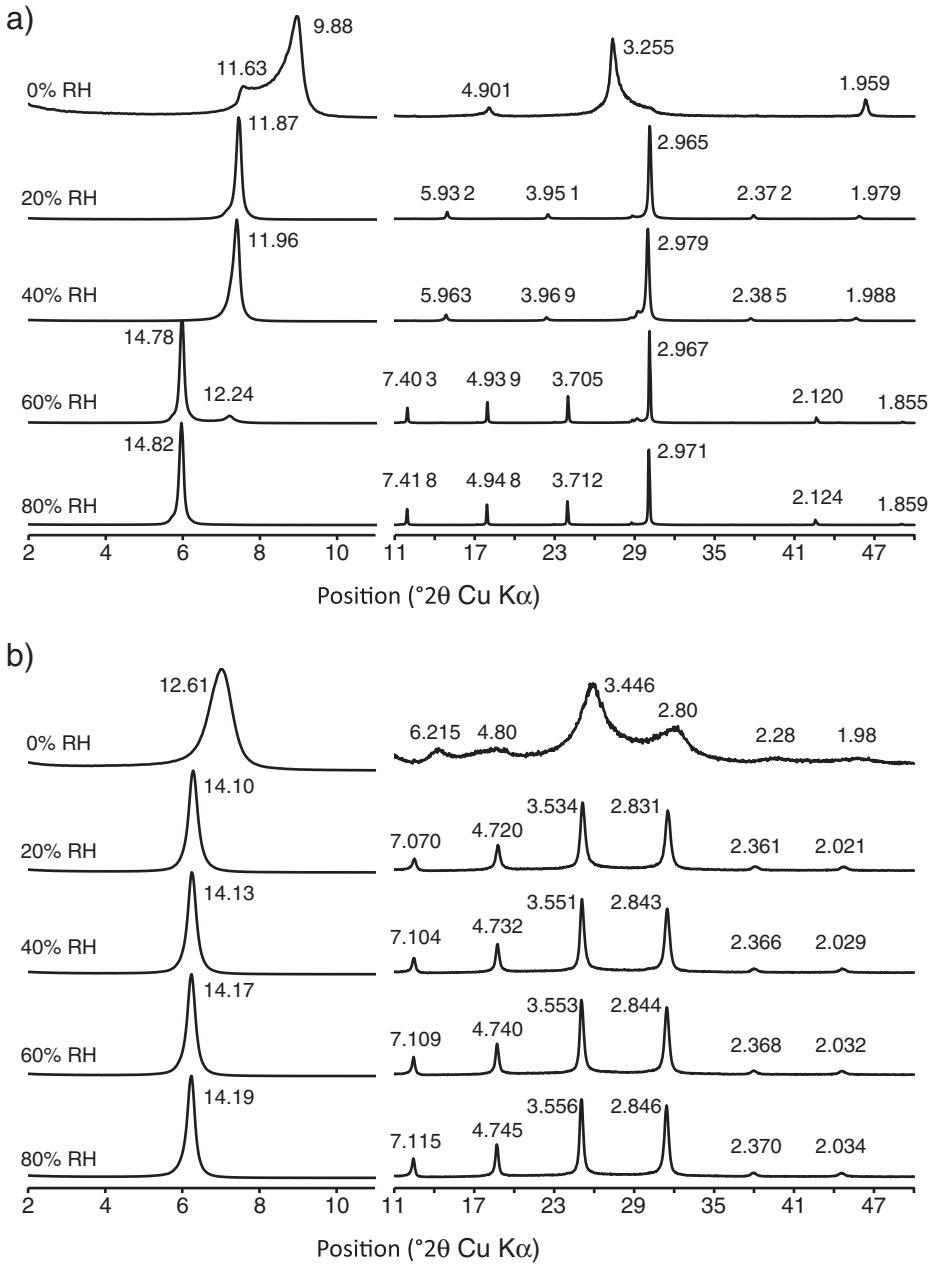

Fig. 2. Evolution of the X-ray diffraction profiles as a function of relative humidity for a) the initial Na-saturated Santa Olalla sample and b) the Na-saturated Santa Olalla sample altered for 672 h. High-angle intensities are scaled up by a 20x factor compared to the 4–11° 2θ angular range.

Table 2
Evolution of basal reflection qualitative describers (position and rationality) as a function of relative humidity for initial and altered samples.

Sample	Santa Olalla		Altered 672 h	
	$d_{(001)}$ (Å)	ξ/X_i	$d_{(001)}$ (Å)	ξ/X_i
~0% (vacuum)	9.81	0.049/4	13.53	0.728/7
20%	11.86	0.006/6	14.14	0.024/7
40%	11.93	0.013/6	14.19	0.029/7
60%	14.82	0.022/7	14.21	0.017/7
80%	14.85	0.019/7	14.22	0.017/7

Notes: The ξ parameter that accounts for the departure from rationality of the 00ℓ reflection series is calculated as the standard deviation of the $\ell \times d_{(00\ell)}$ values calculated for the X_i measurable reflections over the 2–50° 2θ CuKα angular range. For the unaltered Santa Olalla vermiculite, reflections of 1 W vermiculite were omitted for the calculation of the ξ parameter both at 0 and 60% RH.

of the 001 reflection, however. This additional mixed layer is dominated also by 1 W layers but contains minor amounts (<10%) of both 0 W and 2 W layers. Interlayers of 1 W vermiculite host cations and H_2O molecules (5.2 p.f.u.) located at the interlayer mid-plane and characterized by a very limited positional disorder (Debye–Waller factor, B_{wat}, of ~4 Å^2 — Table 3), consistent with high layer charge (Dazas et al., 2015; Ferrage et al., 2005b, 2011).

3.2.2.2. Aluminized vermiculite. Chemical analyses (Table 1) show both a major decrease of the number of alkali cations and presence of non-exchangeable (Al, Fe) cations in the altered vermiculite interlayers compared to original vermiculite, in agreement with results of Mareschal et al. (2009). Consistent with the partial collapse of the structure under vacuum conditions (Fig. 2b), both species coexist in altered interlayers as the total number of interlayer Fe and Al (0.66 p.f.u.) is far to

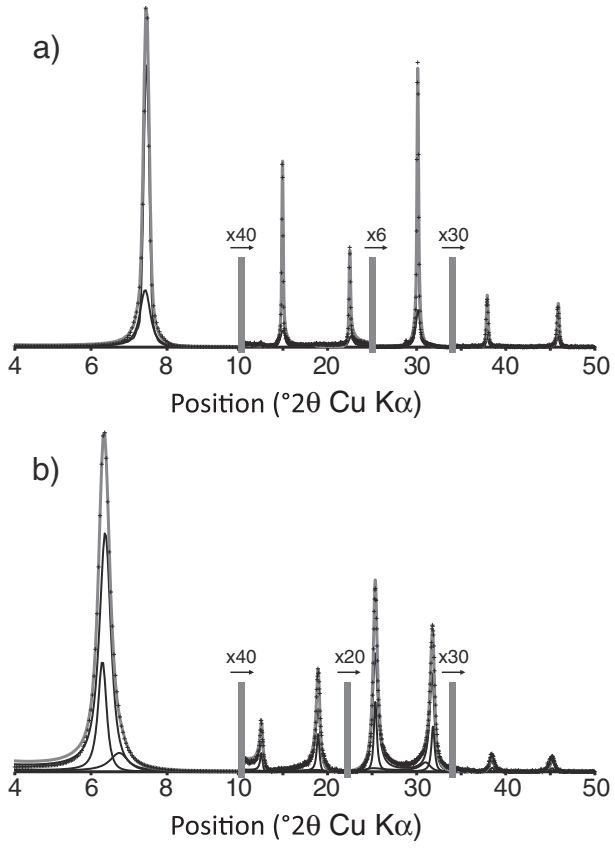

Fig. 3. Modeling of the X-ray diffraction profiles for (a) the initial Na-saturated Santa Olalla sample and (b) the Na-saturated Santa Olalla sample altered for 672 h. XRD data (recorded at 20% RH) is shown as crosses, calculated profile is shown as a solid gray line, and elementary contributions to the diffracted intensity are shown as solid black lines. Gray bars indicate the scaling up of the high-angle region intensities as compared to the 4–10° 2θ angular range.

compose a complete gibbsite-like interlayer sheet (4.0 cations p.f.u.). Despite the apparent rationality of 00ℓ position reflections (Table 2) three mixed layers were required to fit XRD data. Overall, altered vermiculite contains ~88% of HI layers (Table 3). The overwhelming contribution of HI layers provides strong constraints for the determination of a structure model for these layers with a 14.04 Å layer-to-layer distance. In the interlayer configuration leading to the optimum fit shown in Fig. 3b, all interlayer cations (Al, Fe, and Na) are located at the interlayer mid-plane. The number of exchangeable alkali cations was set to match the chemical analysis, whereas that of (Al, Fe) cations was adjusted to ~0.64 Al (p.f.u.). In addition, two planes of H_2O molecules located at a distance of ~1.0 Å on each side of the interlayer mid-plane were considered, each of these planes hosting 4.05 H_2O molecules (p.f.u.) accounting both for H_2O molecules hydrating alkali cations and for hydroxyl groups and H_2O molecules coordinating non-exchangeable (Al, Fe) cations. Note that because X-ray diffraction is only sensitive to the electronic density, it is not possible to differentiate H_2O molecules from hydroxyl groups and only water molecules were considered during the fitting procedure. However and as determined for the monohydrated state, these planes of H_2O molecules present a limited positional disorder (B_{wat} ~7 Å^2) and it can thus be assumed that both H_2O molecules and hydroxyl groups are located at about the same position along the **c***-axis.

3.3. Expandability evolution and structural constraints on the aluminization process

Structural characterization of the two end-members allows using XRD profile modeling to quantify reaction progress as a function of alteration time (Ferrage et al., 2005c). For all samples, XRD patterns recorded at 20% RH are reported as function of alteration time in Fig. 4. These patterns show complex profiles with important asymmetry and peak broadening indicative of the coexistence of various mixed layers. XRD patterns of 60 and 96 h samples appear especially heterogeneous with reflections characteristic of the two end-members. Note that XRD patterns of altered samples were systematically fitted attributing all layers with a layer-to-layer distance close to 14 Å to HI layers. The initial sample presents however some minor contribution of Na-saturated 2 W layers (~3% — Table 3) that could persist in other samples but 2 W layers were not considered owing to (i) the low sensitivity of XRD to discriminate between layers having similar layer-to-layer distance (i.e., HI vs. 2 W layers) and (ii) their minor contribution compared to the overall proportion of ~14 Å layers in all samples except for the 12 h sample (Table 3).

The structure model used to fit the pattern of the 12 h sample is similar to that of the unaltered sample (Fig. 5a, Table 3) and involves a main structure almost periodic (99% of 1 W layers interstratified with 0 W layers — Table 3) which allows reproducing most of the XRD profile. A second structure, more heterogeneous, contains the three types of layers (13, 80 and 7% of 2 W-HI, 1 W and 0 W layers, respectively — Table 3). Compared to the unaltered sample, this second structure contains more 2 W-HI layers to fit the low-angle asymmetry of the 001 reflection (Fig. 5a), although the overall increase of 2 W-HI layer content is limited (3 and 5% for initial and 12 h samples, respectively — Table 3). XRD pattern of the 36 h sample exhibits a more prominent asymmetry of the 001 reflection on its low-angle side together with additional broad reflections at 16.6, 24.0 and 27.8° 2θ (Fig. 5b) and was fitted using three mixed layers (Table 3). The first two are similar to those used for unaltered and 12 h samples although the proportion of HI layers is increased in both mixed layers. In addition, the relative contribution of the HI-rich mixed layer increases at the expense of the essentially monohydrated mixed layer (Table 3). Finally, a third mixed layer composed of 1 W and HI layers in similar proportions with a tendency to ordering ($P_{HI-HI} = 0.10 < W_{HI}$ — Table 3) accounts for additional reflections. Five mixed layers were necessary to fit the XRD pattern of the 60 h sample (Fig. 5c, Table 3). The first three are similar to those present in the 36 h sample although their HI layer contents are systematically increased (Table 3). Similar to the previous sample, the relative contribution of mixed layers enriched in HI layers increases further at the expense of the essentially monohydrated mixed layer (93% of 1 W layers). Two additional mixed layers were introduced in the structure model to account for the presence of a peak at ~14 Å (Fig. 5c). These two randomly interstratified mixed layers contain 68 and 88% of HI layers (Table 3). A similar structure model was used to fit the XRD pattern of 96 h sample (Fig. 5d, Table 3). Compared to the 60 h sample, the proportion of HI layers increases in all five mixed layer contributions. In addition, and consistent with the maximum intensity peak at ~14 Å (Fig. 5d), mixed layers dominated by HI layers prevail in the 96 h sample (Table 3). Compared to the previous sample, the 001 reflection observed at ~14 Å for 168 h sample is sharper, indicative of a HI-dominated structure model, despite the presence of a persistent high-angle asymmetry (Fig. 5e). Consistently, a mixed layer dominated by HI layers (92% HI layers) prevails in the structure model (Table 3) accounting for the almost rational series of basal reflections. A second mixed layer dominated by HI layers (66%) is responsible for the slight high-angle asymmetry of the 001 reflection. The other two mixed layers, whose composition is similar to those in the 96 h sample and dominated by 1 W layers, represent marginal contributions (Table 3) necessary to reproduce the bump on the high-angle side of the 001 reflection as well as the asymmetry observed on the low-angle side of the 005 reflection (at ~30° 2θ — Fig. 5e). Finally, similar structure models allowed fitting 240 and 672 h samples (Figs. 5f and 3b, Table 3). In both samples, the main contribution is a randomly interstratified mixed layer with ~90% HI layers. In addition, an almost periodic HI structure (98% of HI layers — Table 3) allows fitting the sharp tops of 00ℓ reflections, and a third mixed layer

Table 3
Optimum structural parameters used for the simulation of XRD data.

Alteration time	Cont. (%)[a]	2 W or HI/ 1 W/0 W[b]	Reichweite junction probabilities	LLD 2 W-HI[c]	NH_2O 2 W-HI[d]	BH_2O 2 W-HI[d]	LLD 1W[c]	NH_2O 1W[d]	BH_2O 1W[d]	N[e]	σ_z[f]	Total 2 W-HI/1 W/0 W	Rp (6–50)
Sta Olalla (unaltered)	62	0/99/1	R0	14.75*	8.2	4	11.87	5.2	4	100	0.08	2/95/3	8.28%
	38	6/87/7	R0										
12 h	61	0/99/1	R0	14.05	8.1	5	11.88	5.2	4	100	0.08	6/92/3	6.85%
	39	13/80/7	R0										
36 h	43	2/97/1	R0	14.04	8.1	7	11.88	5.2	4	50	0.09	15/83/2	7.01%
	43	20/76/4	R0										
	14	40/60/0	$R1/P_{HI-HI} = 0.10$										
60 h	25	6/93/1	R0	14.05	8.1	7	11.88	5.2	4	30	0.13	36/62/2	6.29%
	42	26/72/2	R0										
	14	68/30/2	R0										
	12	88/10/2	R0										
	7	45/55/0	$R1/P_{HI-HI} = 0.10$										
96 h	11	10/88/2	R0	14.04	8.1	7	11.88	5.2	4	25	0.14	58/40/2	3.01%
	23	32/66/2	R0										
	29	62/36/2	R0										
	33	90/8/2	R0										
	4	48/52/0	$R1/P_{HI-HI} = 0.10$										
168 h	2	10/88/2	R0	14.05	8.1	7	11.88	5.2	4	20	0.16	82/16/2	3.97%
	3	30/68/2	R0										
	26	66/32/2	R0										
	69	92/6/2	R0										
240 h	6	50/48/2	R0	14.00	8.1	7	11.88	5.2	2	18	0.17	88/10/2	2.08%
	72	89/9/2	R0										
	22	98/2/0	R0										
672 h	9	53/44/3	R0	14.04	8.1	7	11.88	5.2	4	15	0.18	88/10/2	2.23%
	68	89/9/2	R0										
	23	98/2/0	R0										

[a] Relative proportion of the different contributions to the diffracted intensity.
[b] Relative proportion of the different layer types in the mixed layers contributing to the diffracted intensity. 2 W, HI, 1 W, and 0 W stand for bi-hydrated, hydroxy-interlayered, mono-hydrated, and de-hydrated layers, respectively.
[c] Layer-to-layer distance (LLD) of the various layer types. LLD of 0 W layers is constant at 9.8 Å.
[d] Number (N), and Debye–Waller thermal factor (B) of H_2O molecules in 2 W and 1 W layers (per $O_{20}(OH)_4$).
[e] Mean size of the coherent scattering domains along the **c***-axis (in layers).
[f] Standard deviation of the LLD parameter (in Å — Ferrage et al., 2005a).

with ~50% 1 W layers accounts for the high- and low-angle asymmetries of the 001 and 005 reflections, respectively (Figs. 5f and 3b, Table 3).

Among other structural parameters, a significant decrease of coherent scattering domain (CSD) size is observed with increasing alteration (N ~100 and 15 layers for initial and most altered samples, respectively — Table 3). The layer-to-layer distance fluctuation (σ_z parameter) is also positively correlated to the overall content of HI layers, although the layer-to-layer distance of the two end-members is about constant for all samples (~14.04 Å and ~11.89 Å for HI and 1 W layers, respectively — Table 3).

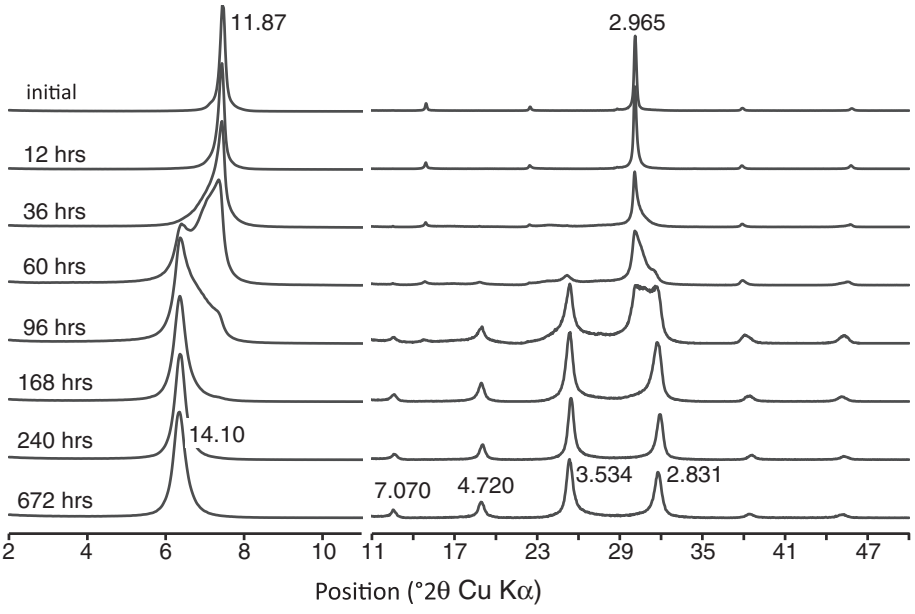

Fig. 4. XRD patterns obtained at 20% RH for Na-saturated Santa Olalla vermiculite samples after contrasting alteration times (initial, 12, 36, 60, 96, 168, 240, and 672 h). High-angle intensities are scaled up by a 20x factor compare to the 2–11 ° 2θ angular range.

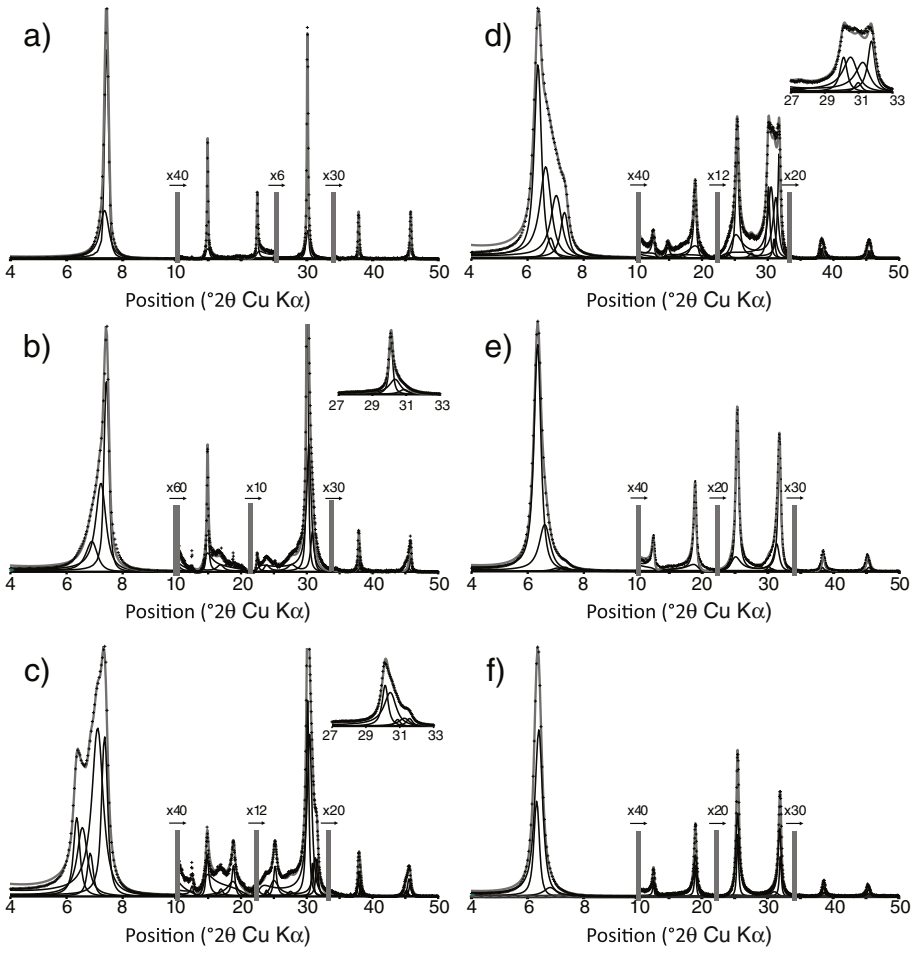

Fig. 5. Modeling of the X-ray diffraction profiles for the Na-saturated Santa Olalla samples altered for (a) 12, (b) 36, (c) 60, (d) 96, (e) 168, and (f) 240 h. All diffraction patterns were collected at 20% RH. Gray bars and patterns as for Fig. 3.

4. Discussion

4.1. Interlayer structure of initial and hydroxy-interlayered vermiculite

With both interlayer cations and H_2O molecules located at the interlayer mid-plane, the interlayer configuration proposed by Moore and Reynolds (1997) for mono-hydrated vermiculite allows fitting XRD data of the initial sample (Fig. 3a), thus confirming the validity of the model (Ferrage et al., 2011). The XRD model incorporates 5.2 H_2O molecules p.f.u., that is ~13% less than the H_2O content determined from TG analysis (~5.9 p.f.u.). Both techniques do not probe however the same H_2O molecules as TG analyses account for both interlayer structural H_2O and H_2O sorbed at the crystal surface, the latter being overlooked by XRD. The number of interlayer H_2O molecules deduced from XRD profile fitting corresponds to ~3.0 H_2O molecules per interlayer cation consistent with previous reports for tetrahedrally substituted high-charge expandable clays in the 1 W state (Dazas et al., 2015; Ferrage et al., 2011).

Chemical analysis of altered vermiculite shows an important decrease of interlayer exchangeable alkali content compared to the initial sample (Table 1), consistent with the CEC decrease determined by Mareschal et al. (2009). Moreover, in agreement with the initial non-stoichiometric dissolution of vermiculite in acidic conditions described by Mareschal et al. (2009) this sample displays the presence of non-exchangeable interlayer (Al, Fe) cations. As a consequence, structure model of the altered vermiculite interlayers is more heterogeneous than that of the initial vermiculite with the coexistence of both exchangeable alkali cations and hydroxy (Al, Fe) cations within the same interlayers, as proposed previously (Dixon and Jackson, 1962; Jackson, 1962; Meunier, 2007). XRD profile modeling indicates indeed the prevalence of HI layers coexisting with a minor proportion of 1 W layers (Table 3), insufficient to host all alkali cations. The presence of hydrated alkali cations within HI layers is supported by the faint variations of altered vermiculite layer-to-layer distance as a function of RH conditions (Fig. 2b — Dazas et al., 2013; Ferrage et al., 2005a, 2007a). The partial collapse of HI layers under secondary vacuum, similar to the collapse commonly observed upon moderate heating (Barnhisel and Bertsch, 1989; Douglas, 1989), supports also the presence of hydrated interlayer cations, as no significant dehydroxylation of hydroxy (Al, Fe) cations is expected under mild temperature conditions or under vacuum. Although it is difficult to derive the actual number of H_2O molecules hydrating interlayer alkali cations, as the associated electron density cannot be differentiated from that of hydroxy (Al, Fe), the weight loss over the 50–250 °C range (Fig. 1, Table 1) indicates the presence of ~3.8 H_2O molecules (p.f.u., 5.8 H_2O molecules per interlayer cation), consistent with the hydration of interlayer Na cations in high-charge 2 W expandable clays (4.6–4.9 H2O molecules per interlayer cation — Skipper et al., 1991; Suzuki et al., 1987) despite the low RH conditions. Accordingly, the layer-to-layer distance of HI layers suggests that two planes of H_2O molecules are associated with interlayer alkali cations. It is then possible to hypothesize that both alkali and (Al, Fe) cations are located at the interlayer mid-plane surrounded by two atomic planes whose electron density accounts for oxygen atoms, hydroxyl groups, and H_2O molecules. To assess the extent of the interlayer gibbsite-like

sheet, electron density both at the interlayer mid-plane and at the two interlayer "water" planes can be varied and the corresponding XRD pattern compared to the data (Fig. 6). Experimental distribution of intensity is satisfactorily fitted with an electron density corresponding to 1.2–1.3 Al + Na (p.f.u.) at the interlayer mid-plane, both cations hosting the same number of electrons. Out of this range, significant mismatches are visible for 002, 003, and 005 reflections (Fig. 6). Taking into account the 0.66 Na p.f.u. (Table 1), hydroxy (Al, Fe) thus accounts for 0.55–0.65 Al at the interlayer mid-plane. This range is consistent with the excess (Al, Fe) present in altered vermiculite interlayers (0.66 p.f.u. — Table 1). HI interlayers thus appear to host gibbsite-like sheets with only ~15% completeness despite the layer-to-layer distance similar to that of chlorite with complete interlayer gibbsite-like sheets, consistent with early reports on natural HI minerals (Dixon and Jackson, 1962) and on synthetic Mg-analogs (Caillère and Hénin, 1949). Note that the σ_z parameter is increased in HI layers compared to unaltered 1 W, indicative of the incomplete and heterogeneous filling of altered vermiculite interlayers (Ferrage et al., 2005d). HI layers partial collapse under secondary vacuum (present study) and upon mild heating (110 °C) of K-saturated samples (Mareschal et al., 2009) is consistent also with such a limited interlayer occupancy by hydroxy (Al, Fe) and HI layers are best depicted as layers for which expandability is reduced by the presence of isolated $Me[(OH)_x,(H_2O)_y]^{3-x}$ islands (with $Me = Al^{+3}$ or Fe^{3+}), as proposed previously (Dixon and Jackson, 1962; Grim and Johns, 1953). The ~14.0–14.1 Å layer-to-layer distance resulting from the presence of these isolated "islands" increases significantly interlayer porosity, especially for RH values below 60% at which the initial Na-saturated vermiculite is essentially monohydrated (Table 2), and could be responsible for an increased water sorption capacity of altered vermiculite compared to initial sample. Finally, it should be noted that hydroxy (Al, Fe) apparently bear ~1.5 positive charges per (Al, Fe) cation to balance layer charge deficit (Table 1). This charge is similar or slightly higher than in previous reports of HI vermiculites (0.8–1.5 — Hsu and Bates, 1964; Veith, 1978). It should be noted however that the latter studies were performed in solutions having much higher OH:Al ratios than those used for the preparation of the present samples (Mareschal et al., 2009), thus inducing logically the formation of larger hydroxy (Al, Fe) cations, as discussed by Rich (1968).

4.2. Evolution of expandability and constraints on reaction mechanisms

XRD profile modeling was successfully applied to all experimental patterns obtained for vermiculite samples as a function of alteration progress, thus confirming the adequacy of the methodology developed by Ferrage et al. (2005c) to characterize structures with variable degree of heterogeneity occurring during a reaction. Relative proportions of the different layer types (unreacted 1 W and HI) are plotted in Fig. 7 as a function of alteration time to evidence the steady hydroxylation of interlayers. This quantitative description highlights that although the vermiculite sample used in this study is well-crystallized, its structure never contains more than 95% of a given layer type, consistent with the intrinsic hydration heterogeneity of swelling clays (Ferrage et al., 2005a, 2007a, 2010). After ~200 h of alteration the structure reaches however a stable composition dominated by HI layers hosting a low number of hydroxylated and non-exchangeable (Al, Fe) interlayer cations. As a result, quantification and structural characterization of HI layers with XRD is a relevant indicator of subtle changes affecting vermiculite interlayer chemistry and especially of hydroxylation of interlayer metal cations. Despite the observed stability of HI layer proportion (Fig. 7), aluminization could still be active at the end of the experiment performed, consistent with the evolution of solution chemistry that indicates a limited but effective incorporation of (Al, Fe) cations from 240–672 h (Mareschal et al., 2009), possibly by increasing the density and/or polymerization of hydroxy (Al, Fe) "islands".

In addition, XRD profile modeling allows determining stacking sequences of the different layer types. The coexistence of randomly interstratified mixed layers with contrasting compositions (relative proportions of elementary layers), as in the present case, indicates an overall segregation of the different layer types. Segregation can be quantitatively described by the Sg index (Cesari et al., 1965; Drits and Tchoubar, 1990; Ferrage et al., 2005c; Dazas et al., 2013):

$$Sg(\mathrm{MW}) = 1 - \frac{1 - \left(\frac{\sum_{i=1}^{n} \left[Ab.\mathrm{ML}^{i} \times \left(\mathrm{W}_{\mathrm{MW}}^{i} \right)^{2} \right]}{\sum_{i=1}^{n} \left[Ab.\mathrm{ML}^{i} \times \left(\mathrm{W}_{\mathrm{MW}}^{i} \right) \right]} \right)}{1 - \sum_{i=1}^{n} \left[Ab.\mathrm{ML}^{i} \times \left(W_{\mathrm{MW}}^{i} \right) \right]} \quad (1)$$

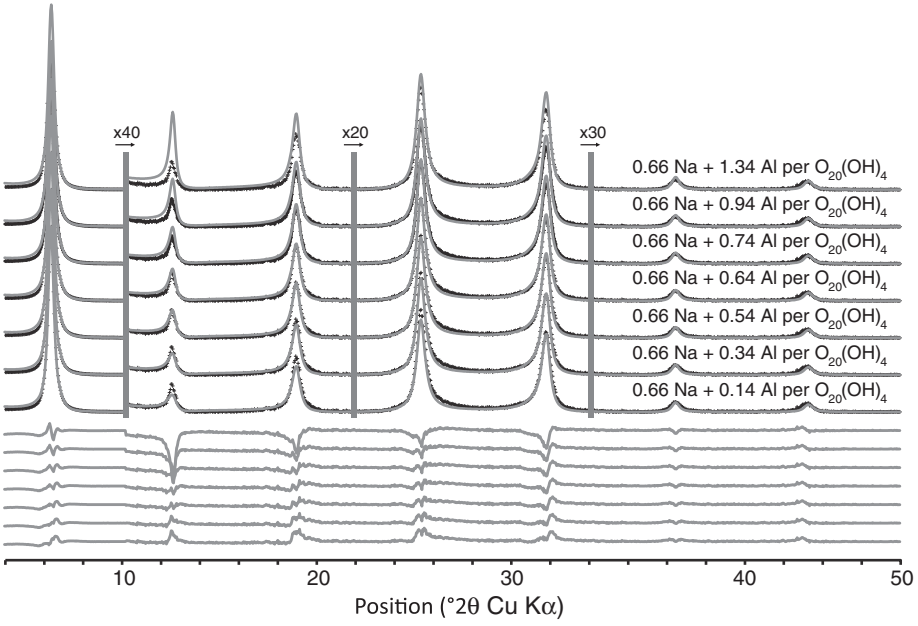

Fig. 6. Sensitivity of calculated X-ray diffraction patterns to the number of interlayer cations. XRD patterns calculated for contrasting numbers of interlayer cations (0.66 Na^{+} and a variable number of Al^{3+} p.f.u. — solid gray line) located at the interlayer mid-plane are compared to the data (crosses). Gray bars as for Fig. 3. Difference plots are shown at the bottom of the figure as solid gray lines.

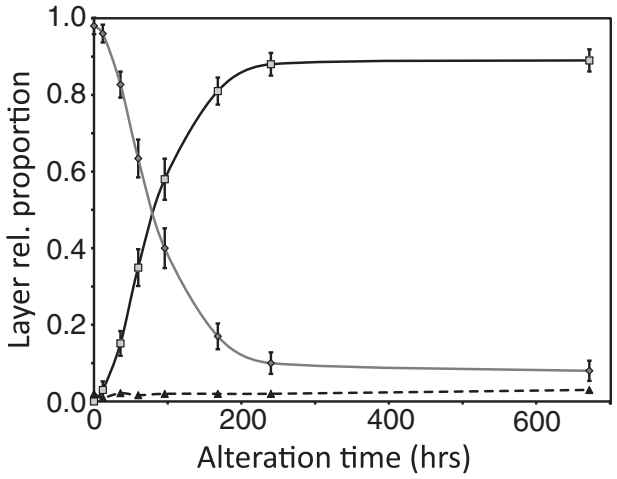

Fig. 7. Relative abundance of the different layer types as a function of alteration time. Uncertainties on relative proportions were calculated as proposed by Ferrage et al. (2007b). Diamonds, squares, and triangles correspond to 1 W (Na), 2 W-HI, and 0 W layers, respectively.

where *Ab*.ML^{i} represents the relative proportion of the *i*th mixed layer contribution, W^{i}_{MW} the relative abundance in this mixed layer of the major layer type in the sample, and *n* the total number of mixed layers. The increase of this index with reaction progress (Fig. 8) could possibly result from the aluminization of vermiculite interlayers starting from the particle edges and steadily progressing towards the particle core. Such a process would lead to a heterogeneous distribution of hydroxy (Al, Fe) "islands" within vermiculite interlayers as proposed by Dixon and Jackson (1962) and Frink (1965) but inconsistent with the observed stability of altered vermiculite composition along the analytical profiles (data not shown). In addition, this process would modify the size of coherent scattering domains (along the **c***-axis) only marginally whereas a significant decrease is deduced from XRD profile modeling. Despite the unfavorable large size of crystals used in the present experimental study, this evolution is rather consistent with the complete aluminization of individual interlayers, as previously reported for cation exchange processes (Ferrage et al., 2005c; Glaeser and Méring, 1954; Iwasaki and Watanabe, 1988; Levy and Francis, 1975; Mamy and Gaultier, 1979; Tertre et al., 2011), and a layer-by-layer transformation leading to the occurrence of segregated domains along the **c***-axis.

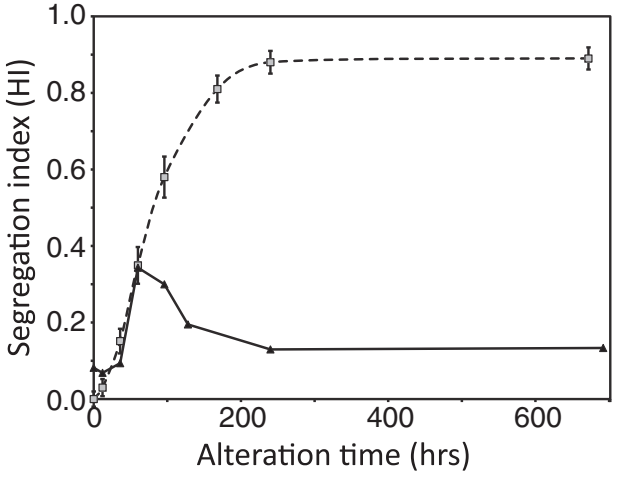

Fig. 8. Segregation index of HI layers (Sg(HI) — solid triangles) as a function of alteration time. Relative abundance of HI layers is shown as gray squares.

Consistently, the maximum Sg index value obtained in the present study (~0.3) is similar to that reported during cation exchange processes (Ferrage et al., 2005c; Tertre et al., 2011) despite the smaller size fractions used in the latter studies (<1–2 μm compared to 200–400 μm in the present case). Finally, a minor ordered (R = 1) mixed layer containing both HI and expandable interlayers was identified during the present aluminization process (Table 3), consistent with previous reports (Barnhisel and Rich, 1966) and supporting the layer-by-layer character of the process.

4.3. Implications for crystal chemistry and reactivity of hydroxy-interlayered soil minerals

As a result of the layer-by-layer aluminization process, the initial Na-saturated Santa Olalla vermiculite is transformed to a heterogeneous mixed layer by the steady incorporation of hydroxy (Al, Fe) cations in vermiculite interlayers (Table 3, Fig. 8). The resulting structure model differs strongly however from the widely accepted description of HI minerals as a solid solution between expandable 2:1 clay and aluminous chlorite end-members (Barnhisel and Bertsch, 1989). The latter model assumes a homogeneous crystal chemistry of hydroxy interlayers, whose occupancy essentially depends on aluminization progress. Contrastingly, the mixed layer model of HI vermiculite described in the present study is consistent with that proposed by Meunier (2007) to account for XRD patterns obtained from HI minerals upon various treatments (ethylene glycol solvation, heating, …). In the latter model, expandable 2:1 layers and aluminous chlorite layers with a partial interlayer filling are randomly interstratified to form HI minerals.

This alternative model for HI minerals bears significant implications as to their reactivity, and more especially as to the observed CEC decrease with aluminization progress. In the present case, a CEC reduction of several tens of cmolc·kg^{-1} corresponds to several mg·g^{-1} of (Al, Fe) cations extracted with the tricitrate method (Mareschal et al., 2009), the latter value being about one order of magnitude lower than those reported for a variety of minerals and a similar CEC decrease by Barnhisel and Bertsch (1989), thus exceeding the possible discrepancy between extractible and actual contents of interlayer (Al, Fe) cations. Higher OH:Al ratios and pH conditions used in cited works (Barnhisel and Bertsch, 1989) favor the formation of large interlayer hydroxy-Al cations and possibly account for this difference. Results of Mareschal et al. (2009) indicate consistently that a similar decrease of CEC can be induced by a low number of small high-charge hydroxy (Al, Fe) cations or by a high number of larger low-charge hydroxy-Al cations. As a consequence, the amount of (Al, Fe) cations extracted or fixed cannot be used as an absolute estimate of the CEC reduction. Its evolution during a given experiment remains however a valid indicator of aluminization progress.

In the present study, extractible (Al, Fe) content is linearly correlated with the number of HI layers (Fig. 9A), thus indicating that all HI layers react in a similar way to the tricitrate extraction method along the aluminization experiment. As a result, CEC decrease reported by Mareschal et al. (2009) can be correlated to HI layer content (Fig. 9B). CEC of the 12 h sample is similar to that of the initial sample despite the presence of ~5% of HI layers. Contrastingly, CEC decrease is most effective for contents of HI layers ranging from 5–65%. From 65–90% HI layers, CEC decreases at a much reduced rate to reach ~15% of the initial CEC when experimental aluminization reaches a steady state. Although remaining expandable layers (~10% — Table 3) can account for part of this CEC, HI layers most likely contribute also owing to their alkali cation content (Table 1). Finally, one can note that HI layers formed during the late stage of the aluminization process do not induce a significant CEC decrease. In the present work, all HI layers possess however a similar behavior with respect to interlayer (Al, Fe) extraction. The possible origin for the persistence of unreacted vermiculite layers at the end of the experiment remains similarly unclear.

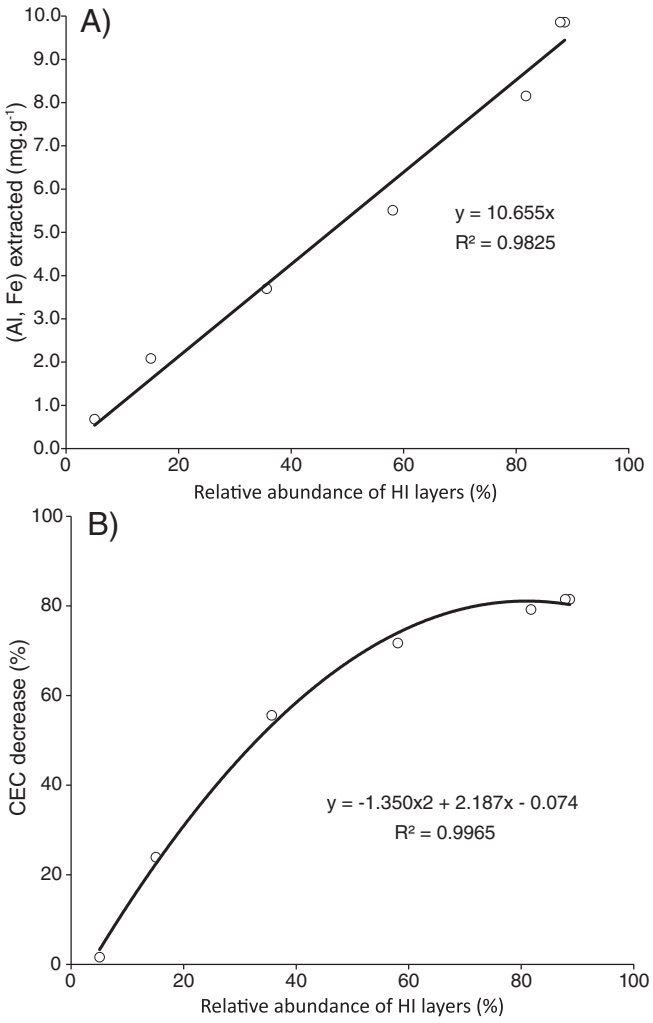

Fig. 9. Extractible (Al, Fe) content measured with the tricitrate method (A) and CEC decrease (B) as a function of HI layers relative proportion. Extractible (Al, Fe) and CEC values from Mareschal et al. (2009).

5. Conclusions

Results from the present study are consistent with the description of HI minerals as mixed layers with expandable 2:1 layers randomly interstratified with aluminous chlorite layers having a partial interlayer filling (HI layers) rather than as members of a solid solution between expandable 2:1 clay and aluminous chlorite end-members (Barnhisel and Bertsch, 1989). Interlayer hydroxy (Al, Fe) cations form isolated islands in all HI layers, leading to gibbsite-like interlayer sheets with a marginal completeness of ~15% and coexisting together with a minor number of hydrated alkali cations. They enforce also a layer-to-layer distance of ~14 Å that remains stable under a wide range of relative humidity conditions but that can collapse, at least partially, under mild temperature or secondary vacuum conditions. The ~14 Å layer-to-layer distance induces in turn the presence of a high number of H_2O molecules hydrating alkali cations despite the reduced number of the latter, these numbers being reduced by 35 and 60% compared to the original 1 W vermiculite, respectively. A major outcome of this mixed layer model is that CEC decrease induced by aluminization is correlated to the overall content of HI layers in the mixed layers rather than to the steady increase of interlayer occupancy by gibbsite-like sheets.

Although self-aluminization of swelling clay minerals has been reported to mimic natural processes in acidic soils (Vicente et al., 1977), relevance of both the proposed structure model and the layer-by-layer aluminization process to natural soils is to be assessed as present experimental OH:Al ratios are extremely low. The charge of Al complexes formed is apparently close to 1.5+, consistent with previous experiments however, and possibly with natural conditions favorable to aluminization of expandable clay interlayers. Heterogeneity of clay mineral assemblages reported along the aluminization process, with various mixed layer contributions of contrasting compositions and ordering, appears however common both in experimental studies (Barnhisel and Rich, 1966) and natural acidic soils (Viennet et al., 2015) despite contrasting aluminization conditions.

Acknowledgments

Financial support from the French National Program EC2CO-Biohefect to the CLAIE project (IC2MP/ISTerre) is gratefully acknowledged. ISTerre is part of Labex OSUG@2020 (ANR10 LABX56).

References

Argüelles, A., Leoni, M., Blanco, J.A., Marcos, C., 2010. Semi-ordered crystalline structure of the Santa Olalla vermiculite inferred from X-ray powder diffraction. Am. Mineral. 95, 126–134.
Bain, D.C., Mellor, A., Wilson, M.J., 1990. Nature and origin of an aluminous vermiculitic weathering product in acid soils from upland catchments in Scotland. Clay Miner. 25, 467–475.
Barnhisel, R.I., Bertsch, P.M., 1989. Chlorites and hydroxy-interlayered vermiculite and smectite. In: Dixon, J.B., Weed, S.B. (Eds.), Minerals in Soil Environments. Soil Science Society of America, Madison, WI, pp. 729–788.
Barnhisel, R.I., Rich, C.I., 1966. Preferential hydroxyaluminum interlayering in montmorillonite and vermiculite. Soil Sci. Soc. Am. J. 30, 35–39.
Bortoluzzi, E.C., Velde, B., Pernes, M., Dur, J.C., Tessier, D., 2008. Vermiculite, with hydroxy-aluminium interlayer, and kaolinite formation in a subtropical sandy soil from south Brazil. Clay Miner. 43, 185–193.
Brindley, G.W., Sempels, R.E., 1977. Preparation and properties of some hydroxy-aluminium beidellites. Clay Miner. 12, 229–237.
Caillère, S., Hénin, S., 1949. Experimental formation of chlorites from montmorillonite. Mineral. Mag. 28, 612–620.
Carstea, D.D., 1968. Formation of Hydroxy-Al and -Fe interlayers in montmorillonite and vermiculite: influence of particle size and temperature. Clay Clay Miner. 16, 231–238.
Cesari, M., Morelli, G.L., Favretto, L., 1965. The determination of the type of stacking in mixed-layer clay minerals. Acta Crystallogr. 18, 189–196.
Cradwick, P.D., Wilson, M.J., 1978. Calculated X-ray diffraction curves for the interpretation of a three-component interstratified system. Clay Miner. 13, 53–65.
Dazas, B., Lanson, B., Breu, J., Robert, J.L., Pelletier, M., Ferrage, E., 2013. Smectite fluorination and its impact on interlayer water content and structure: a way to fine tune the hydrophilicity of clay surfaces? Microporous Mesoporous Mater. 181, 233–247.
Dazas, B., Ferrage, E., Delville, A., Lanson, B., 2014. Interlayer structure model of trihydrated low-charge smectite by X-ray diffraction and Monte Carlo modeling in the Grand Canonical ensemble Micropor. Am. Mineral. 97, 1724–1735.
Dazas, B., Lanson, B., Delville, A., Robert, J.-L., Komarneni, S., Michot, L.J., Ferrage, E., 2015. Influence of tetrahedral layer charge on the organization of interlayer water and ions in synthetic Na-saturated smectites. J. Phys. Chem. C 119, 4158–4172.
de la Calle, C., Suquet, H., 1988. Vermiculite. In: Bailey, S.W. (Ed.), Hydrous phyllosilicates (exclusive of micas). Reviews in Mineralogy vol. 19. Mineralogical Society of America, Chantilly, Va, pp. 455–496.
de la Calle, C., Suquet, H., Dubernat, J., Pezerat, H., 1978. Mode d'empilement des feuillets dans les vermiculites hydratées à "deux couches". Clay Miner. 13, 275–297.
Dixon, J.B., Jackson, M.L., 1962. Properties of intergradient chlorite-expansible layer silicates of soils. Soil Sci. Soc. Am. J. 26, 358–362.
Douglas, L.A., 1989. Vermiculites. In: Dixon, J.B., Weed, S.B. (Eds.), Minerals in Soil Environments. Soil Science Society of America, Madison, WI, pp. 635–728.
Drits, V.A., Sakharov, B.A., 1976. X-ray Structure Analysis of Mixed-layer Minerals. Nauka, Moscow.
Drits, V.A., Tchoubar, C., 1990. X-ray Diffraction by Disordered Lamellar Structures: Theory and Applications to Microdivided Silicates and Carbons. Springer-Verlag, Berlin.
Drits, V.A., Sakharov, B.A., Lindgreen, H., Salyn, A., 1997a. Sequential structure transformation of illite-smectite-vermiculite during diagenesis of Upper Jurassic shales from the North Sea and Denmark. Clay Miner. 32, 351–371.
Drits, V.A., Srodon, J., Eberl, D.D., 1997b. XRD measurement of mean crystallite tickness of illite and illite/smectite: reappraisal of the Kubler index and the Scherrer equation. Clay Clay Miner. 45, 461–475.
Egli, M., Fitze, P., Mirabella, A., 2001. Weathering and evolution of soils formed on granitic, glacial deposits: results from chronosequences of Swiss alpine environments. Catena 45, 19–47.
Egli, M., Mirabella, A., Sartori, G., Fitze, P., 2003. Weathering rates as a function of climate: results from a climosequence of the Val Genova (Trentino, Italian Alps). Geoderma 111, 99–121.
Egli, M., Mirabella, A., Sartori, G., Giaccai, D., Zanelli, R., Plötze, M., 2007. Effect of slope aspect on transformation of clay minerals in Alpine soils. Clay Miner. 42, 373–398.
Ferrage, E., Lanson, B., Malikova, N., Plancon, A., Sakharov, B.A., Drits, V.A., 2005a. New insights on the distribution of interlayer water in bi-hydrated smectite from X-ray diffraction profile modeling of 00l reflections. Chem. Mater. 17, 3499–3512.

Ferrage, E., Lanson, B., Sakharov, B.A., Drits, V.A., 2005b. Investigation of smectite hydration properties by modeling experimental X-ray diffraction patterns: part I. Montmorillonite hydration properties. Am. Mineral. 90, 1358–1374.
Ferrage, E., Tournassat, C., Rinnert, E., Charlet, L., Lanson, B., 2005c. Experimental evidence for Ca-chloride ion pairs in the interlayer of montmorillonite. An XRD profile modeling approach. Clay Clay Miner. 53, 348–360.
Ferrage, E., Tournassat, C., Rinnert, E., Lanson, B., 2005d. Influence of pH on the interlayer cationic composition and hydration state of Ca-montmorillonite: analytical chemistry, chemical modelling and XRD profile modelling study. Geochim. Cosmochim. Acta 69, 2797–2812.
Ferrage, E., Kirk, C.A., Cressey, G., Cuadros, J., 2007a. Dehydration of Ca-montmorillonite at the crystal scale. Part I: structure evolution. Am. Mineral. 92, 994–1006.
Ferrage, E., Lanson, B., Sakharov, B.A., Geoffroy, N., Jacquot, E., Drits, V.A., 2007b. Investigation of dioctahedral smectite hydration properties by modeling of X-ray diffraction profiles: influence of layer charge and charge location. Am. Mineral. 92, 1731–1743.
Ferrage, E., Lanson, B., Michot, L.J., Robert, J.L., 2010. Hydration properties and interlayer organization of water and ions in synthetic Na-smectite with tetrahedral layer charge. Part 1. Results from X-ray diffraction profile modeling. J. Phys. Chem. C 114, 4515–4526.
Ferrage, E., Sakharov, B.A., Michot, L.J., Delville, A., Bauer, A., Lanson, B., Grangeon, S., Frapper, G., Jimenez-Ruiz, M., Cuello, G.J., 2011. Hydration properties and interlayer organization of water and ions in synthetic Na-smectite with tetrahedral layer charge. Part 2. Towards a precise coupling between molecular simulations and diffraction data. J. Phys. Chem. C 115, 1867–1881.
Frink, C.R., 1965. Characterization of aluminum interlayers in soil clays. Soil Sci. Soc. Am. J. 29, 379–382.
Glaeser, R., Méring, J., 1954. Isothermes d'hydratation des montmorillonites bi-ioniques (Ca, Na). Clay Min. Bull. 2, 188–193.
Grim, R.E., Johns, W.D., 1953. Clay mineral investigation of sediments in the Northern Gulf of Mexico. Clay Clay Miner. 2, 81–103.
Guinier, A., 1964. Théorie et technique de la radiocristallographie. Dunod, Paris.
Howard, S.A., Preston, K.D., 1989. Profile fitting of powder diffraction patterns. In: Bish, D.L., Post, J.E. (Eds.), Modern Powder Diffraction. Reviews in Mineralogy vol. 20. Mineralogical Society of America, Chantilly, Va, pp. 217–275.
Hsu, P.H., Bates, T.F., 1964. Fixation of hydroxy-aluminum polymers by vermiculite. Soil Sci. Soc. Am. J. 28, 763–769.
Iwasaki, T., Watanabe, T., 1988. Distribution of Ca and Na ions in dioctahedral smectites and interstratified dioctahedral mica/smectites. Clay Clay Miner. 36, 73–82.
Jackson, M.L., 1962. Interlayering of expansible layer silicates in soils by chemical weathering. Clay Clay Miner. 11, 29–46.
Levy, R., Francis, C.W., 1975. Demixing of sodium and calcium ions in montmorillonite crystallites. Clay Clay Miner. 23, 475–476.
Mamy, J., Gaultier, J.-P., 1979. Etude comparée de l'évolution des montmorillonites biioniques K–Ca de Camp-Berteaux et du Wyoming sous l'effet des cycles d'humectation et de dessication. Clay Miner. 14, 181–192.
Mareschal, L., Ranger, J., Turpault, M.P., 2009. Stoichiometry of a dissolution reaction of a trioctahedral vermiculite at pH 2.7. Geochim. Cosmochim. Acta 73, 307–319.
Meunier, A., 2007. Soil hydroxy-interlayered minerals: a re-interpretation of their crystallochemical properties. Clay Clay Miner. 55, 380–388.
Moore, D.M., Reynolds Jr., R.C., 1997. X-ray Diffraction and the Identification and Analysis of Clay Minerals. Oxford University Press, Oxford.
Pons, C.H., Pozzuoli, A., Rausell-Colom, J.A., De la Calle, C., 1989. Mécanisme de passage de l'état hydraté à une couche à l'état "zéro couche" d'une vermiculite-Li de Santa-Olalla. Clay Miner. 24, 479–493.
Pret, D., Sammartino, S., Beaufort, D., Meunier, A., Fialin, M., Michot, L.J., 2010. A new method for quantitative petrography based on image processing of chemical element maps: part I. Mineral mapping applied to compacted bentonites. Am. Mineral. 95, 1379–1388.
Rich, C.I., 1960. Aluminium in interlayers of vermiculite. Soil Sci. Soc. Am. J. 24, 26–32.
Rich, C.I., 1968. Hydroxy interlayers in expansible layer silicates. Clay Clay Miner. 16, 15–30.
Righi, D., 1993. Characterization of hydroxy-interlayered vermiculite and illite/smectite interstratified minerals from the weathering of chlorite in a cryorthod. Clay Clay Miner. 41, 484–495.
Righi, D., Meunier, A., 1991. Characterization and genetic interpretation of clays in an acid brown soil (dystrochrept) developed in a granitic saprolite. Clay Clay Miner. 39, 519–530.
Righi, D., Girault, P., Meunier, A., 1986. Transformations des phyllosilicates dans un sol cryptopodzolique humifère du Plateau de Millevaches, France. Clay Miner. 21, 43–54.
Sakharov, B.A., Drits, V.A., 1973. Mixed-layer kaolinite-montmorillonite: a comparison of observed and calculated diffraction patterns. Clay Clay Miner. 21, 15–17.
Sakharov, B.A., Lanson, B., 2013. X-ray identification of mixed-layer structures. Modelling of diffraction effects. In: Bergaya, F., Lagaly, G. (Eds.), Handbook of Clay Science vol. B. Elsevier, pp. 51–135.
Sakharov, B.A., Naumov, A.S., Drits, V.A., 1982a. X-ray diffraction by mixed-layer structures with random distribution of stacking faults. Dokl. Akad. Nauk 265, 339–343 (in Russian).
Sakharov, B.A., Naumov, A.S., Drits, V.A., 1982b. X-ray intensities scattered by layer structures with short-range ordering parameters $S \geq 1$ and $G \geq 1$. Dokl. Akad. Nauk 265, 871–874 (in Russian).
Sakharov, B.A., Naumov, A.S., Drits, V.A., 1983. X-ray scattering by defect layer structures. Kristallografia 28, 951–958 (in Russian).
Sakharov, B.A., Lindgreen, H., Salyn, A., Drits, V.A., 1999a. Determination of illite-smectite structures using multispecimen X-ray diffraction profile fitting. Clay Clay Miner. 47, 555–566.
Sakharov, B.A., Lindgreen, H., Salyn, A.L., Drits, V.A., 1999b. Mixed-layer kaolinite-illite-vermiculite in North Sea shales. Clay Miner. 34, 333–344.
Sato, T., Watanabe, T., Otsuka, R., 1992. Effects of layer charge, charge location, and energy change on expansion properties of dioctahedral smectites. Clay Clay Miner. 40, 103–113.
Sawhney, B.L., 1968. Aluminium interlayers in layer silicates effect of ratio Al solution, time of reaction, and type of structure. Clay Clay Miner. 16, 157–163.
Schwertmann, U., Jackson, M.L., 1964. Influence of hydroxy aluminium ions on pH titration curves of hydrogen-aluminium clays. Soil Sci. Soc. Am. J. 28, 179–183.
Skipper, N.T., Soper, A.K., Mc Connell, J.D.C., 1991. The structure of interlayer water in vermiculite. J. Chem. Phys. 94, 5751–5760.
Suzuki, M., Wada, N., Hines, D.R., Wittingham, M.S., 1987. Hydration states and phase transitions in vermiculite intercalation compounds. Phys. Rev. B36, 2844–2851.
Tertre, E., Ferrage, E., Bihannic, I., Michot, L.J., Prêt, D., 2011. Influence of the ionic strength and solid/solution ratio on Ca(II)-for-Na^+ exchange on montmorillonite. Part 2: understanding the effect of the m/V ratio. Implications for pore water composition and element transport in natural media. J. Colloid Interface Sci. 363, 334–347.
Tolpeshta, I.I., Sokolova, T.A., Bonifacio, E., Falcone, G., 2010. Pedogenic chlorites in podzolic soils with different intensities of hydromorphism: origin, properties, and conditions of their formation. Eurasian Soil Sci. 43, 777–787.
Veith, J.A., 1978. Selectivity and adsorption capacity of smectite and vermiculite for aluminum of varying basicity. Clay Clay Miner. 26, 45–50.
Vicente, M.A., Razzaghe, M., Robert, M., 1977. Formation of aluminium hydroxy vermiculite (intergrade) and smectite from mica under acidic conditions. Clay Miner. 12, 101–112.
Viennet, J.-C., Hubert, F., Ferrage, E., Tertre, E., Legout, A., Turpault, M.-P., 2015. Investigation of clay mineralogy in a temperate acidic soil of a forest using X-ray diffraction profile modeling: beyond the HIS and HIV description. Geoderma 241–242, 75–86.
Wilson, M.J., 1966. The weathering of biotite in some Aberdeenshire soils. Mineral. Mag. 35, 1080–1093.
Wilson, M.J., Bain, D.C., Duthie, D.M.L., 1984. The soil clays of Great Britain; II, Scotland. Clay Miner. 19, 709–735.